ARMY RESEARCH LABORATORY

Improved Dispersion of a Fin-Stabilized Projectile Using a Passive Moveable Nose

by Mark Costello and Raditya Agarwalla

ARL-CR-464 **April 2001**

prepared by

Mark Costello and Raditya Agarwalla
Oregon State University
Department of Mechanical Engineering
Corvallis, Oregon 97331

under contract

DAAD17-00-P-0853

Army Research Laboratory
Aberdeen Proving Ground, MD 21005-5066

ARL-CR-464 **April 2001**

Improved Dispersion of a Fin-Stabilized Projectile Using a Passive Moveable Nose

Mark Costello and Raditya Agarwalla
Oregon State University

Abstract

A key and often quoted metric associated with gun systems is impact point accuracy. The extent of impact dispersion is a complex function of a battery of parameters, including gun geometry and tolerances, the fire control system, projectile manufacturing tolerances, etc. The work reported here investigates potential impact point accuracy improvement for a penetrator-type projectile realized by replacing the rigid nose cone wind screen with a passive gimballed nose. By comparing the impact point dispersion of a rigid projectile with a similar gimballed nose projectile, it is shown that impact point accuracy can be significantly improved. For the example penetrator projectile considered, impact point dispersion is reduced by more than 50%.

Contents

INTENTIONALLY LEFT BLANK.

List of Figures

INTENTIONALLY LEFT BLANK.

List of Tables

INTENTIONALLY LEFT BLANK.

1. Introduction

The merit of a penetrator is often assessed by a relatively short list of metrics that typically includes parameters such as terminal velocity, penetrator weight, cost, system accuracy, etc. Of these parameters, system accuracy is usually near the top of the list in terms of importance, and it is of significant concern during weapon system development. Given two identical weapon systems with the exception of accuracy, the system with superior accuracy enjoys a distinct advantage on the battlefield. A system with improved accuracy can engage targets at a greater range and obtain the same probability of hit, providing the tank commander with increased flexibility during an engagement. Alternatively, a system with better accuracy will register more first-volley hits at the same range, reducing the counter fire threat. Furthermore, a gun system with superior accuracy ultimately requires fewer shots to achieve mission objectives, hence inducing less burden on the logistics pipeline.

The initial state of a projectile as it exits the gun muzzle and enters free flight can be viewed as a random process. The random nature of the initial free flight state stems from many effects, but perhaps most notably from gun tube and projectile manufacturing tolerances combined with the resulting gun tube and projectile vibration. As the projectile flies down range, these uncertainties, along with aerodynamic disturbances along the trajectory, map into dispersion at the target. Designers can take two basic approaches toward improving accuracy; they can reduce the variability of projectile initial free flight conditions or reduce the sensitivity of the projectile trajectory to initial free flight conditions. One way to attack this problem using the latter approach is to replace the rigid wind screen with a passive gimballed nose. If the pivot point of the nose section is forward of the nose aerodynamic center, then the nose will tend to rotate into the relative wind and subsequently reduce aerodynamic jump caused by projectile normal force. A passive gimballed nose projectile is an attractive design modification because it is a relatively simple mechanism that requires no active electronic controls. Furthermore, for many penetrator designs, the nose cone is empty and could easily house the gimbal joint.

Early in the development of controlled rockets, the notion of utilizing a moveable nose to actively control the trajectory of a projectile was established [1]. Goddard obtained a patent titled “An Apparatus for Steering Aircraft” which outlined the basic concept. More recently, Barrett and Stutts [2] further developed this concept and subsequently developed and tested a gun-launched, actively controlled nose. The moveable nose concept has also been investigated in unguided projectile applications as well. Krantz [3] obtained a patent for a telescopic passive nose on a high velocity aerodynamic body. Schmidt and Donovan [4] developed a simple closed form solution for an effective C_{La} and C_{Ma} for a moveable nose projectile configuration that is based on projectile linear theory [5]. A limited number of prototype projectiles were fired, and range data was reduced to estimate aerodynamic coefficients. The work reported herein extends the previous work mentioned by simulating the exterior ballistics of a gimballed nose

projectile in atmospheric flight and subsequently comparing impact point dispersion statistics with a similarly-sized rigid projectile. The gimbaled nose projectile dynamic model includes the typical six degrees of freedom for the main body plus an additional three degrees of freedom for the rotation of the nose with respect to the main body. Impact point dispersion statistics are generated through Monte Carlo simulation of the initial pitch and yaw rates of the projectile.

2. Gimbal Nose Projectile Dynamic Model

A schematic of the gimballed nose projectile configuration is shown in Figure 1. The gimballed nose projectile consists of forward and aft projectile sections. The configuration possesses three position degrees of freedom, which are the inertial position components of the mass center of the composite body described in an inertial reference frame.

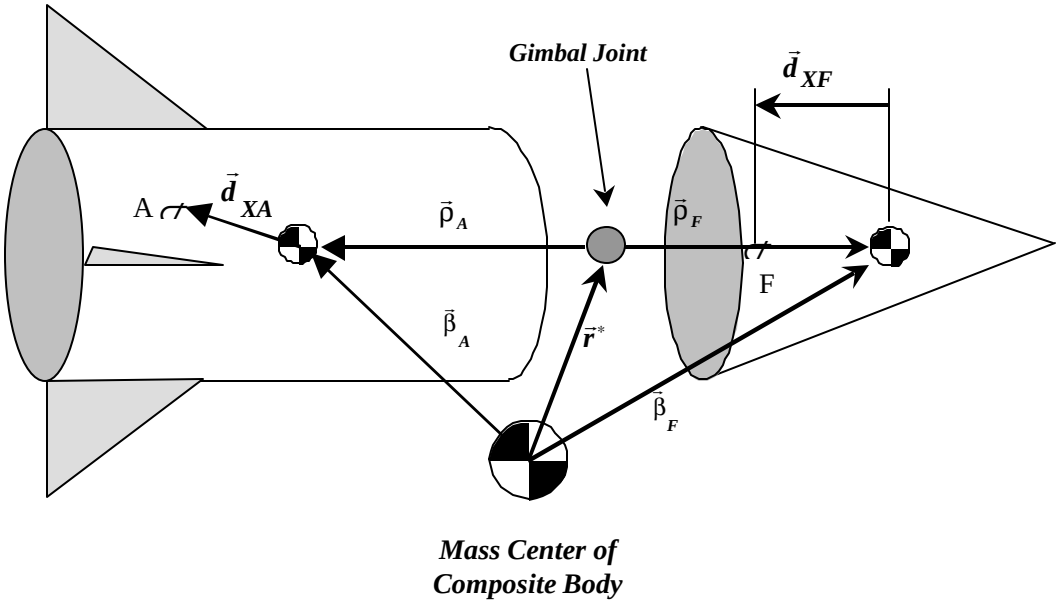

Figure 1. Schematic of the gimballed nose projectile configuration.

$$\vec{r}_{O\to\oplus} = x\vec{i}_I + y\vec{j}_I + z\vec{k}_I . \tag{1}$$

A total of six degrees of freedom describe the aft and forward body orientation. The orientation of the aft projectile is obtained through a sequence of three body-fixed rotations. Starting from an inertial coordinate system, the aft body is successively rotated through Euler yaw, pitch, and roll angles to arrive at its final orientation in space. The forward body orientation is also obtained by a sequence of three body-fixed rotations. Starting from the aft body reference frame, the forward body is successively rotated through Euler yaw, pitch, and roll angles to arrive at its final orientation in space. With these definitions, a rigid projectile configuration is realized

when the forward-body Euler angles are zero, $f_F = q_F = y_F = 0$.

As shown in equation 2, the velocity vector components of the mass center of the composite body are defined in the aft body reference frame.

$$\vec{v}_{\oplus/I} = u\vec{i}_A + v\vec{j}_A + w\vec{k}_A. \tag{2}$$

With the definitions given in equations 1 and 2, the resulting translational kinematic differential equations are given by equation 3.

$$\begin{Bmatrix} \dot{x} \\ \dot{y} \\ \dot{z} \end{Bmatrix} = \begin{bmatrix} T_A \end{bmatrix} \begin{Bmatrix} u \\ v \\ w \end{Bmatrix}. \tag{3}$$

Equation 3 contains the transformation matrix from the aft body reference frame to the inertial reference frame, which is provided as equation 4. As shown in equation 5, the transformation from the forward body reference frame to the aft body reference frame takes on the same form as equation 4, except the angles are the nose angles.

$$T_A = \begin{bmatrix} c_{q_A} c_{y_A} & s_{f_A} s_{q_A} c_{y_A} - c_{f_A} s_{y_A} & c_{f_A} s_{q_A} c_{y_A} + s_{f_A} s_{y_A} \\ c_{q_A} s_{y_A} & s_{f_A} s_{q_A} s_{y_A} + c_{f_A} c_{y_A} & c_{f_A} s_{q_A} s_{y_A} - s_{f_A} c_{y_A} \\ -s_{q_A} & s_{f_A} c_{q_A} & c_{f_A} c_{q_A} \end{bmatrix}. \tag{4}$$

$$T_F = \begin{bmatrix} c_{q_F} c_{y_F} & s_{f_F} s_{q_F} c_{y_F} - c_{f_F} s_{y_F} & c_{f_F} s_{q_F} c_{y_F} + s_{f_F} s_{y_F} \\ c_{q_F} s_{y_F} & s_{f_F} s_{q_F} s_{y_F} + c_{f_F} c_{y_F} & c_{f_F} s_{q_F} s_{y_F} - s_{f_F} c_{y_F} \\ -s_{q_F} & s_{f_F} c_{q_F} & c_{f_F} c_{q_F} \end{bmatrix}. \tag{5}$$

The angular velocity vector expressions for the aft and forward bodies with respect to an inertial reference frame are provided in equations 6 and 7, respectively.

$$\vec{w}_{A/I} = p_A\vec{i}_A + q_A j_A + r_A\vec{k}_A. \tag{6}$$

$$\vec{w}_{F/I} = p_F\vec{i}_F + q_F j_F + r_F\vec{k}_F. \tag{7}$$

With these definitions, the rotational kinematic differential equations are given by equations 8 and 9.

$$\begin{Bmatrix} \dot{f}_A \\ q_A \\ \dot{y}_A \end{Bmatrix} = \begin{bmatrix} 1 & s_{f_A} t_{q_A} & c_{f_A} t_{q_A} \\ 0 & c_{f_A} & -s_{f_A} \\ 0 & s_{f_A} / c_{q_A} & c_{f_A} / c_{q_A} \end{bmatrix} \begin{Bmatrix} p_A \\ q_A \\ r_A \end{Bmatrix}. \tag{8}$$

$$\begin{Bmatrix} \dot{f}_F \\ \dot{q}_F \\ \dot{y}_F \end{Bmatrix} = \begin{bmatrix} 1 & s_{f_F} t_{q_F} & c_{f_F} t_{q_F} \\ 0 & c_{f_F} & -s_{f_F} \\ 0 & s_{f_F} / c_{q_F} & c_{f_F} / c_{q_F} \end{bmatrix} \begin{Bmatrix} p_F \\ q_F \\ r_F \end{Bmatrix} - \begin{bmatrix} c_{y_F} / c_{q_F} & s_{y_F} / c_{q_F} & 0 \\ -s_{y_F} & c_{y_F} & 0 \\ c_{y_F} t_{q_F} & s_{y_F} t_{q_F} & 1 \end{bmatrix} \begin{Bmatrix} p_A \\ q_A \\ r_A \end{Bmatrix}. \tag{9}$$

The translation dynamic equations for the mass center of the composite body are given by equation 10.

$$\begin{Bmatrix} \dot{u} \\ \dot{v} \\ \dot{w} \end{Bmatrix} = \begin{bmatrix} 0 & r_A & -q_A \\ -r_A & 0 & p_A \\ q_A & -p_A & 0 \end{bmatrix} \begin{Bmatrix} u \\ v \\ w \end{Bmatrix} + \frac{1}{m_A + m_F} \begin{Bmatrix} X \\ Y \\ Z \end{Bmatrix}. \tag{10}$$

In equation 10, the first term on the right hand side utilizes the aft body angular velocity components in the cross product operator since the composite body mass center velocity components are defined in the aft body reference frame. The total applied force vector components are given in the aft body reference frame.

The rotational dynamics of the forward and aft projectile sections are derived by first splitting the system at the gimbal joint, which exposes the constraint forces and moments at the joint. As shown in equation 11, by subtracting the force balance of both bodies, the components of the constraint force in the aft body coordinate system can be written in terms of the rotational state variables and their derivatives.

$$\begin{Bmatrix} X_C \\ Y_C \\ Z_C \end{Bmatrix} = A_A \begin{Bmatrix} \dot{p}_A \\ \dot{q}_A \\ \dot{r}_A \end{Bmatrix} + A_F \begin{Bmatrix} \dot{p}_F \\ \dot{q}_F \\ \dot{r}_F \end{Bmatrix} + \{B_{AF}\}, \tag{11}$$

where

$$A_A = \frac{m_A m_F}{m_A + m_F} S_{r_A}, \tag{12}$$

$$A_F = \frac{m_A m_F}{m_A + m_F} T_F S_{r_F}, \tag{13}$$

$$B_{AF} = \frac{m_F}{m_A + m_F}\begin{Bmatrix} X_A \\ Y_A \\ Z_A \end{Bmatrix} - \frac{m_A}{m_A + m_F} T_F \begin{Bmatrix} X_F \\ Y_F \\ Z_F \end{Bmatrix} +$$

$$\frac{m_A m_F}{m_A + m_F} S_{\omega_A} S_{\omega_A} \begin{Bmatrix} \rho_{A_X} \\ \rho_{A_Y} \\ \rho_{A_Z} \end{Bmatrix} -$$

$$T_F S_{\omega_F} S_{\omega_F} \begin{Bmatrix} \rho_{F_X} \\ \rho_{F_Y} \\ \rho_{F_Z} \end{Bmatrix}, \tag{14}$$

$$S_{r_A} = \begin{bmatrix} 0 & -r_{A_Z} & r_{A_Y} \\ r_{A_Z} & 0 & -r_{A_X} \\ -r_{A_Y} & r_{A_X} & 0 \end{bmatrix}, \tag{15}$$

$$S_{r_F} = \begin{bmatrix} 0 & -r_{F_Z} & r_{F_Y} \\ r_{F_Z} & 0 & -r_{F_X} \\ -r_{F_Y} & r_{F_X} & 0 \end{bmatrix}, \tag{16}$$

$$S_{\tilde{r}_F} = \begin{bmatrix} 0 & -\tilde{r}_{F_Z} & \tilde{r}_{F_Y} \\ \tilde{r}_{F_Z} & 0 & -\tilde{r}_{F_X} \\ -\tilde{r}_{F_Y} & \tilde{r}_{F_X} & 0 \end{bmatrix}, \tag{17}$$

$$S_{w_A} = \begin{bmatrix} 0 & -r_A & q_A \\ r_A & 0 & -p_A \\ -q_A & p_A & 0 \end{bmatrix}, \tag{18}$$

and

$$S_{w_F} = \begin{bmatrix} 0 & -r_F & q_F \\ r_F & 0 & -p_F \\ -q_F & p_F & 0 \end{bmatrix}. \tag{19}$$

The constraint moment at the gimbal joint is generated by friction in the joint and potentially by geometric interference between the nose and main projectile body when the total angle between the nose and projectile axes of symmetry exceeds a specific value. Gimbal joint friction is modeled as viscous damping. The gimbal joint friction constraint moment is proportional to the difference in angular velocity between the two projectile body components. Geometric interference is modeled as a stiff linear torsion spring with dead band. The dead band region corresponds to the rotational envelope of the nose with respect to the main projectile body. The gimbal nose geometric interference constraint moment magnitude is proportional to the angle between $\vec{i}_A$ and $\vec{i}_F$, denoted as a_g, and is computed using equation 20.

$$a_g = \cos^{-1}(\cos q_F \cos y_F). \tag{20}$$

The direction of this moment is perpendicular to the plane formed by $\vec{i}_A$ and $\vec{i}_F$. Equation 21 provides an expression for the gimbal joint constraint moment.

$$\begin{Bmatrix} L_C \\ M_C \\ N_C \end{Bmatrix} = K_g \frac{M_g}{\sqrt{\sin^2(q_F) + \cos^2(q_F)\sin^2(y_F)}} \begin{Bmatrix} 0 \\ -\sin(q_F) \\ -\cos(q_F)\sin(y_F) \end{Bmatrix} + C_g \begin{Bmatrix} dp \\ dq \\ dr \end{Bmatrix}, \tag{21}$$

where

$$M_g \begin{cases} 0 & \text{if } \alpha_g \le \alpha^* \\ K_g(\alpha_g - \alpha^*) & \text{if } \alpha_g > \alpha^*, \end{cases} \tag{22}$$

and

$$\begin{Bmatrix} dp \\ dq \\ dr \end{Bmatrix} = \begin{Bmatrix} p_A \\ q_A \\ r_A \end{Bmatrix} - [T_F] \begin{Bmatrix} p_F \\ q_F \\ r_F \end{Bmatrix}. \tag{23}$$

The first term in equation 21 is the geometric interference constraint moment, while the second term represents the friction constraint moment. Notice that when $\vec{i}_A$ and $\vec{i}_F$ are aligned $(a_g = 0)$, the interference constraint moment is singular. Fortunately, this

singularity is avoided since the gimbal joint interference constraint moment is zero in this case.

The rotational dynamic equations of the aft and forward projectile bodies are given by equations 24 and 25, respectively.

$$I_A \begin{Bmatrix} \dot{p}_A \\ \dot{q}_A \\ \dot{r}_A \end{Bmatrix} + S_{w_A} I_A \begin{Bmatrix} p_A \\ q_A \\ r_A \end{Bmatrix} = -\begin{Bmatrix} L_C \\ M_C \\ N_C \end{Bmatrix} + \begin{Bmatrix} L_A \\ M_A \\ N_A \end{Bmatrix} + S_{r_A} \begin{Bmatrix} X_C \\ Y_C \\ Z_C \end{Bmatrix}. \tag{24}$$

$$T_F I_F \begin{Bmatrix} \dot{p}_F \\ \dot{q}_F \\ \dot{r}_F \end{Bmatrix} + T_F S_{w_F} I_F \begin{Bmatrix} p_F \\ q_F \\ r_F \end{Bmatrix} = \begin{Bmatrix} L_C \\ M_C \\ N_C \end{Bmatrix} + T_F \begin{Bmatrix} L_F \\ M_F \\ N_F \end{Bmatrix} - T_F S_{\tilde{r}_F} \begin{Bmatrix} X_C \\ Y_C \\ Z_C \end{Bmatrix}. \tag{25}$$

By substituting the constraint force and moment expressions into equations 24 and 25, the final form of the rotational dynamic equations is obtained and expressed in equation 26.

$$\begin{bmatrix} I_A - S_{r_A} A_A & -S_{r_A} A_F \\ T_F S_{\tilde{r}_F} A_A & T_F I_F + T_F S_{\tilde{r}_F} A_F \end{bmatrix} \begin{Bmatrix} \dot{p}_A \\ \dot{q}_A \\ \dot{r}_A \\ \dot{p}_F \\ \dot{q}_F \\ \dot{r}_F \end{Bmatrix} = \begin{Bmatrix} g_{A_X} \\ g_{A_Y} \\ g_{A_Z} \\ g_{F_X} \\ g_{F_Y} \\ g_{F_Z} \end{Bmatrix}, \tag{26}$$

where

$$\{g_A\} = -S_{w_A} I_A \begin{Bmatrix} p_A \\ q_A \\ r_A \end{Bmatrix} - \begin{Bmatrix} L_C \\ M_C \\ N_C \end{Bmatrix} + \begin{Bmatrix} L_A \\ M_A \\ N_A \end{Bmatrix} + S_{r_A} \{B_{AF}\}, \tag{27}$$

and

$$\{g_F\} = -T_F S_{w_F} I_F \begin{Bmatrix} p_F \\ q_F \\ r_F \end{Bmatrix} + \begin{Bmatrix} L_C \\ M_C \\ N_C \end{Bmatrix} + T_F \begin{Bmatrix} L_F \\ M_F \\ N_F \end{Bmatrix} - T_F S_{\tilde{r}_F} \{B_{AF}\}. \tag{28}$$

Collectively, equations 3, 8, 9, 10, and 26 constitute the gimbal nose projectile dynamic model.

The total external load acting on the composite body is due to weight and steady aerodynamic forces on both the forward and aft body projectile components. The

weight force components in the aft body reference frame is given by equation 29.

$$\begin{Bmatrix} X_G \\ Y_G \\ Z_G \end{Bmatrix} = (m_A + m_F) g \begin{Bmatrix} -s_{q_A} \\ c_{q_A} s_{f_A} \\ c_{q_A} c_{f_A} \end{Bmatrix}. \tag{29}$$

The steady aerodynamic force on the aft body is provided by equation 30.

$$\begin{Bmatrix} X_A \\ Y_A \\ Z_A \end{Bmatrix} = -\frac{1}{2} r \left(\frac{pD^2}{4} \right) \begin{Bmatrix} \left(C_{XO}^A + C_{X2}^A \frac{v^2 + w^2}{\sqrt{u^2 + v^2 + w^2}} \right) \left(u^2 + v^2 + w^2 \right) \\ C_{N_a}^A v \sqrt{u^2 + v^2 + w^2} \\ C_{N_a}^A w \sqrt{u^2 + v^2 + w^2} \end{Bmatrix}. \tag{30}$$

Expressions for the forward body aerodynamic forces take on the same form as equation 30. Aerodynamic coefficients in equation 30 depend on local Mach number at the projectile mass center and are computed using linear interpolation from tabulated data.

The right-hand side terms in equation 26 contain the external moments acting on each section of the projectile. These equations contain contributions from steady and unsteady aerodynamics. The steady aerodynamic moments are computed for each individual body with a cross product between the steady body aerodynamic force vector and the distance vector from the center of gravity to the center of pressure. The unsteady body aerodynamic moments provide a damping source for projectile angular motion and are given for the forward body by equation 31.

$$\begin{Bmatrix} L_{UA}^F \\ M_{UA}^F \\ N_{UA}^F \end{Bmatrix} = \tilde{q}_a D \begin{Bmatrix} C_{DD}^F + \frac{p_F D C_{LP}^F}{2V} \\ \frac{q_F D C_{MQ}^F}{2V} \\ \frac{r_F D C_{NR}^F}{2V} \end{Bmatrix}, \tag{31}$$

where

$$\tilde{q}_a = \frac{1}{8} \rho \left(u^2 + v^2 + w^2 \right) \pi D^2 .$$

The expression for the aft section takes on similar form. Air density is computed using the center of gravity position of the projectile in concert with the standard atmosphere [6]. Finally, the total aerodynamic angle of attack of the aft section is defined in equation 32.

$$a_A = \tan^{-1} \left(\frac{\sqrt{v^2 + w^2}}{u} \right). \tag{32}$$

The aerodynamic angle of attack of the forward body is computed in the same manner, except the velocity components are first converted to the forward body reference frame.

3. Results

The equations of motion for the nine degree-of-freedom gimbal nose projectile model discussed, and a six degree-of-freedom rigid projectile model [6] were numerically integrated to obtain simulated impact points at 1 km, 2 km, and 3 km. The equations of motion were integrated using a fourth-order Runge-Kutta scheme with a time step of 0.000001 s. The physical properties of the projectile are provided in Table 1. Table 2 shows the nominal launch conditions of the projectile.

Table 1. Baseline configuration properties.

Physical Parameter	Value
Total Projectile Mass	3.16688 Kg
Aft-to-total mass ratio	0.99
Aft Roll Inertia	0.00065 slug.ft^2 (1.36 Kg.m^2)
Aft Pitch and Yaw Inertia	0.033 slug.ft^2 (0.045 Kg.m^2)
Aft Length Dimension	0.34 m
Aft Reference Diameter	0.037 m
Forward Roll Inertia	4.2e-6 slug.ft^2 (5.69e-6 Kg.m^2)
Forward Pitch and Yaw Inertia	2.5e-5 slug.ft^2 (3.39e-5 Kg.m^2)
Forward Length Dimension	0.13 m
Forward Reference Diameter	0.04 m
Torsional Spring Constant	99,000 lbf.ft / rad
Torsional Spring Damper	0.00 N.sec
$C_{N_a}^F$	2.00
Gimbal Joint Location	0.38 m

Figure 2, 3, and 4 show position traces vs. time under baseline launch conditions. This trajectory is typical for a cannon-launched tank projectile. Both the rigid and gimballed nose projectiles follow a similar path with small differences not notable when viewing the entire trajectory. Figure 5 plots the velocity of the mass center of the rigid and gimbal nose projectiles over the baseline trajectory. The total velocity decays from a launch speed of 5,590 ft / s to a speed of 2,470 ft / s at 3-km range. The roll rate of the aft section of the gimbal nose projectile and the roll rate of the rigid projectile are shown in Figure 6. Because the aft body of the gimbal nose projectile has slightly lower roll inertia than the rigid projectile and the gimbal friction is zero, the rigid projectile roll rate is slightly less than the aft section of the gimbal nose projectile. The Euler pitch and yaw angles of the aft main projectile body are compared to the rigid projectile Euler pitch and yaw angles in Figures 7 and 8, while the Euler pitch and yaw angles of the nose section are plotted in Figures 9 and 10. Because the nose section inertia properties are smaller than the main projectile body, it oscillates at a notably higher frequency. Both the nose

and main projectile sections angular motion is well behaved, with maximum oscillation under 1°.

Dispersion at the target was created through Monte Carlo simulation of the initial pitch and yaw rate of the projectile. The initial pitch and yaw rates were modeled as independent Gaussian random variables with a mean of zero and standard deviation

Table 2. Nominal initial conditions.Table 3. Nominal initial conditions.

Parameter	Value
x	5.4 m
y	6.6e-6 m
z	-0.001 m
u	1703.6 m / s
v	0.13 m / s
w	-0.9 m / s
y_A	3.0°
q_A	5.0°
f_A	0.0°
p_A	0.0 deg / s
q_A	60.7° / s
r_A	-0.8° / s
y_F	0.0°
q_F	0.0°
f_F	0.0°
p_F	0.0° / s
q_F	60.7° / s
r_F	-0.8° / s

of 3 rad/s. A sample size of 50 simulations was used in computing impact point dispersion statistics. Figures 11–13 show the Monte Carlo simulation impact points for the baseline rigid and gimbal nose projectile configurations at a range of 1 km, 2 km, and 3 km, respectively. In all the charts, the large circles correspond to a region such that 66% of the shot impacts fall within the circle. The large dashed circle corresponds to the rigid projectile, while the small solid circle corresponds to the gimbal nose configuration. The dispersion circle radii for the rigid projectile at 1 km, 2 km, and 3 km is 1.1 m, 2.2 m, and 3.3 m, while the dispersion circle radii for the gimbal nose projectile at 1 km, 2 km, and 3 km is 0.5 m, 0.9 m, and 1.4 m, respectively. Notice that the mean impact point of the two projectile configurations is different. The ratio of the dispersion circle radius for the gimbal nose to rigid projectile configuration is 0.43, and it is independent of range. Thus, for the example penetrator projectile equipped with a gimbal nose, dispersion at any range can be reduced by a factor of 0.43.

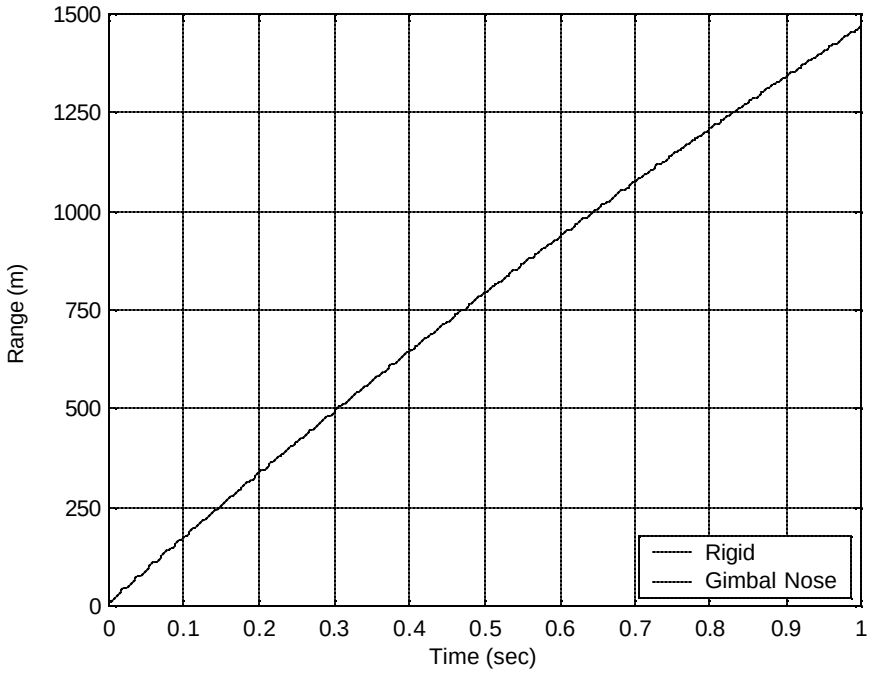

Figure 2. Range vs. time.

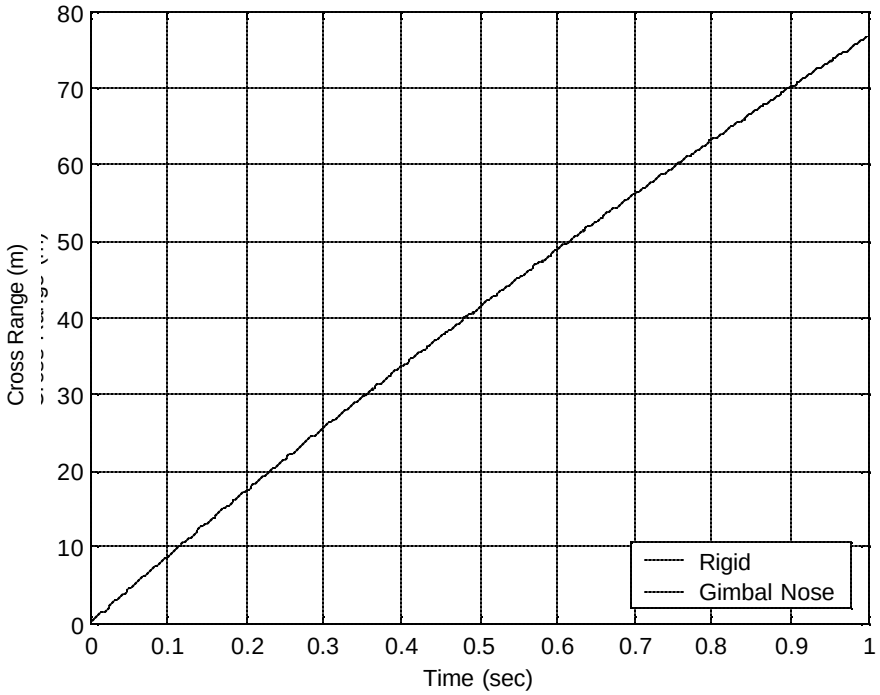

Figure 3. Cross range vs. time

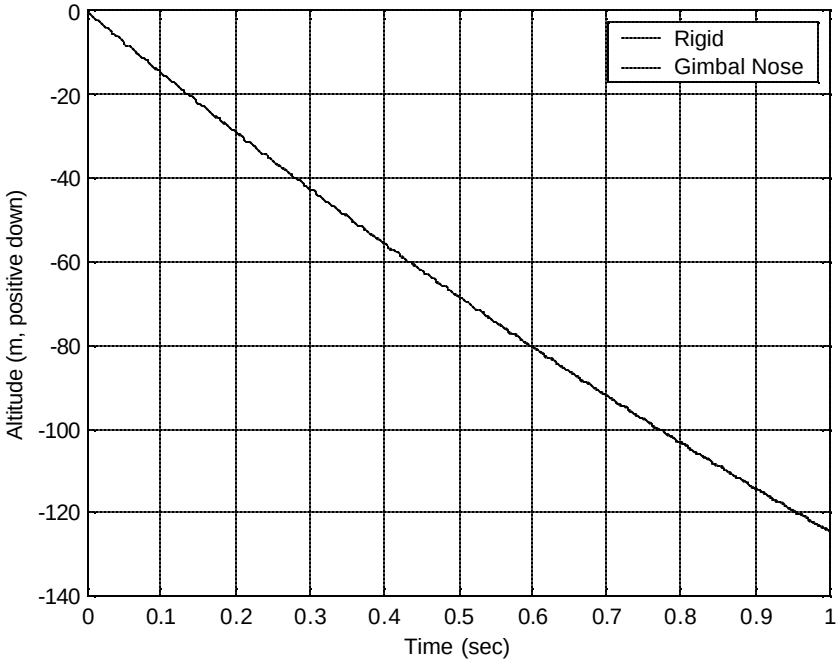

Figure 4. Altitude vs. time.

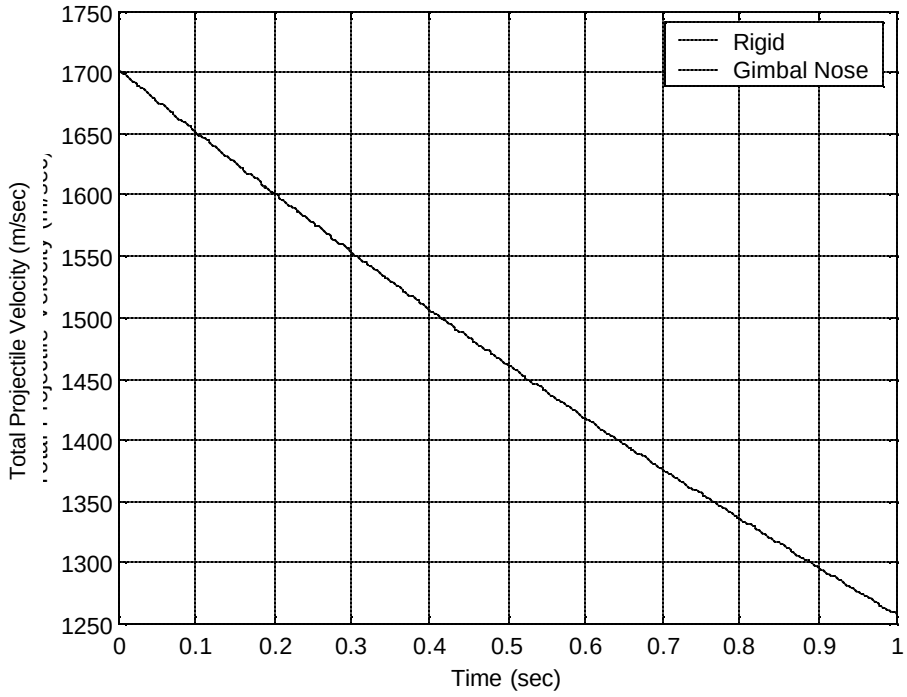

Figure 5. Total velocity vs. time.

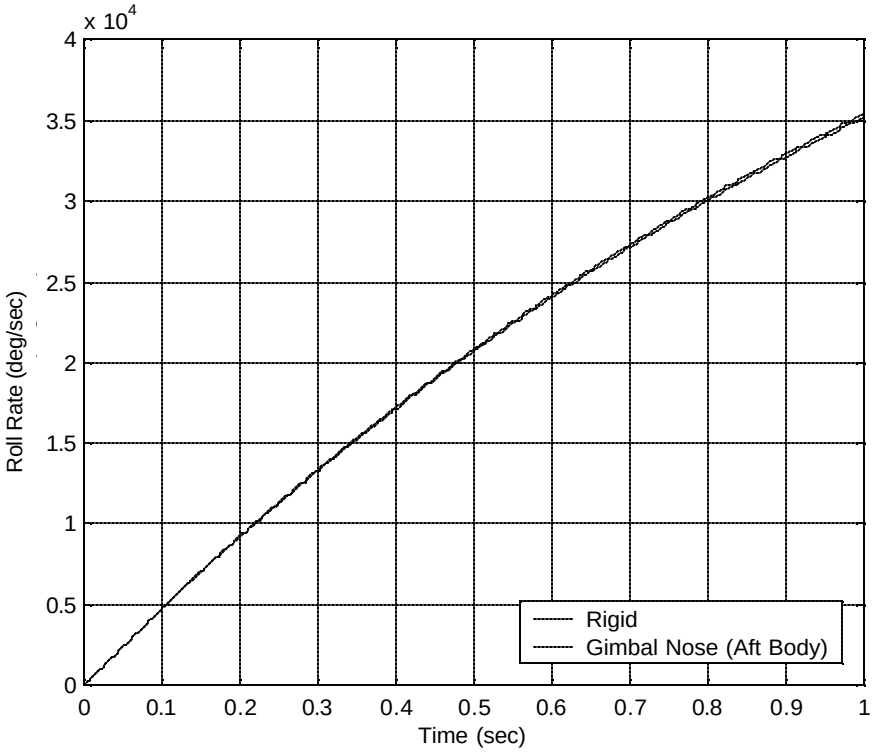

Figure 6. Roll rate vs. time.

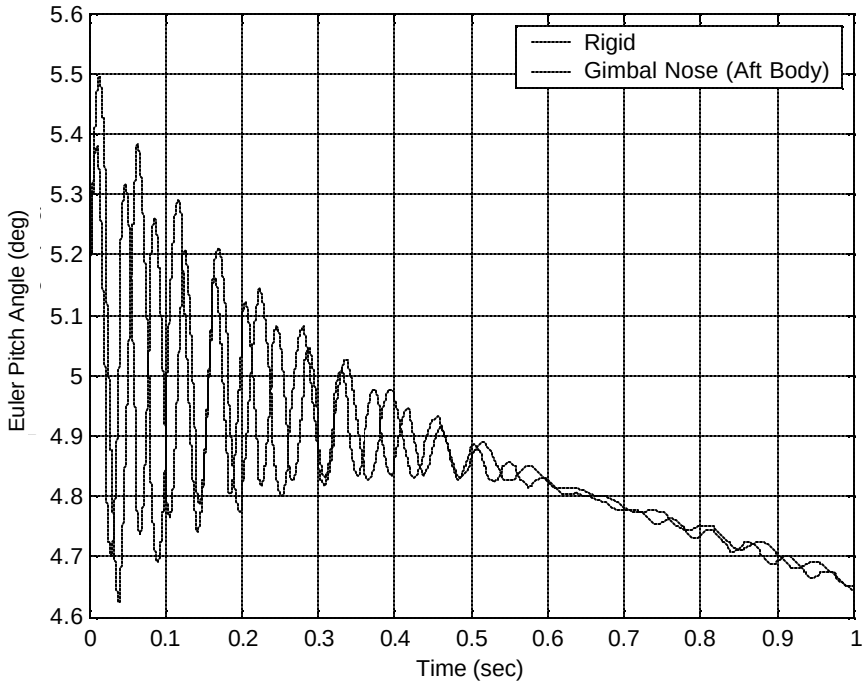

Figure 7. Euler pitch angle vs. time.

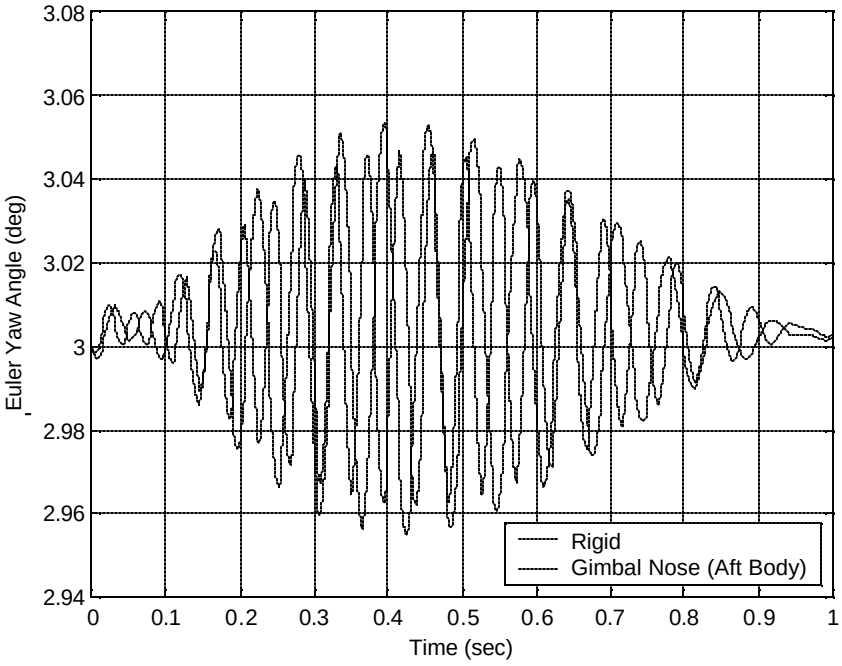

Figure 8. Euler yaw angle vs. time.

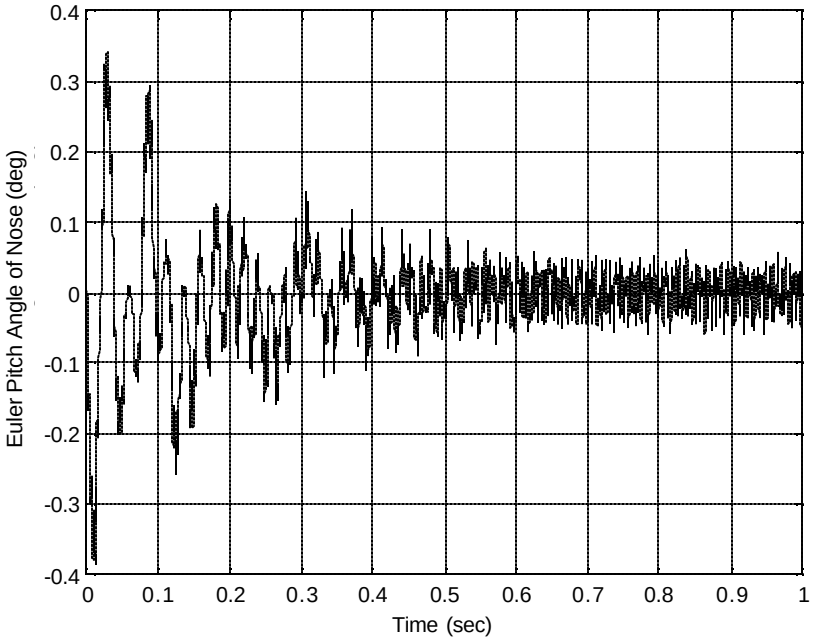

Figure 9. Euler pitch angle of nose vs. time.

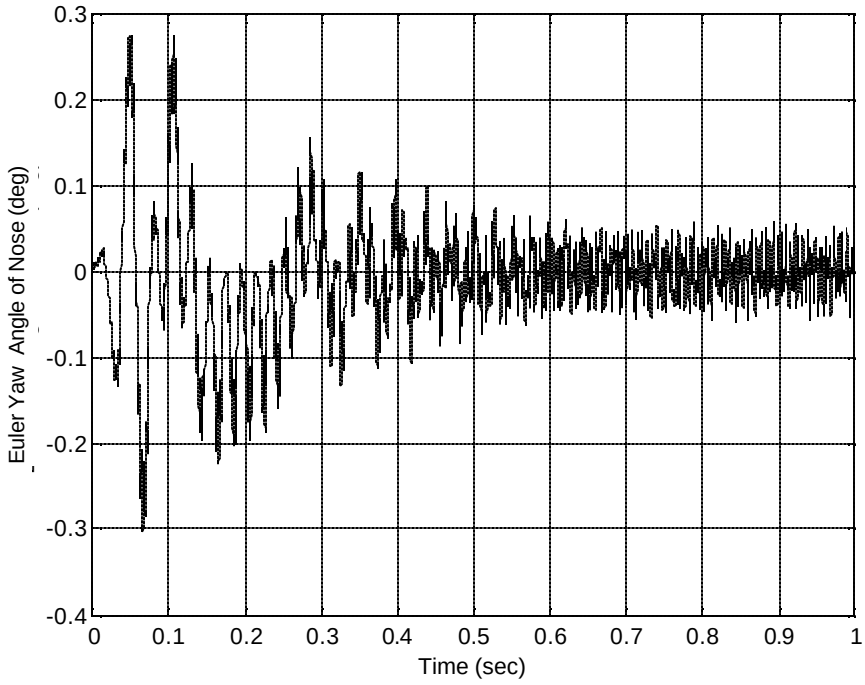

Figure 10. Euler yaw angle of nose vs. time.

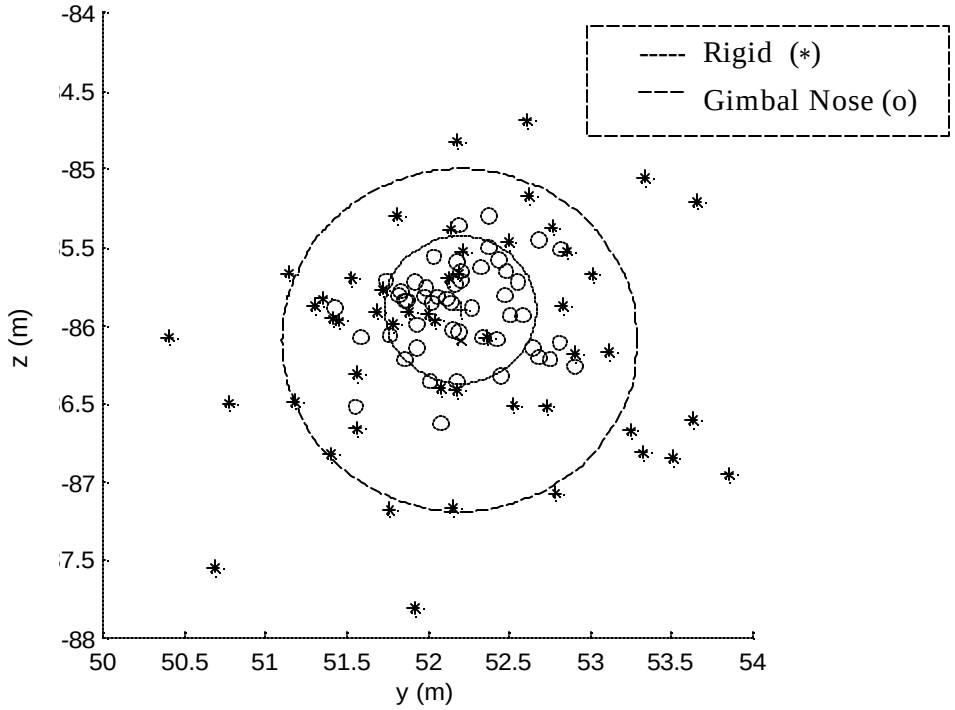

Figure 11. Impact point dispersion at 1 km range.

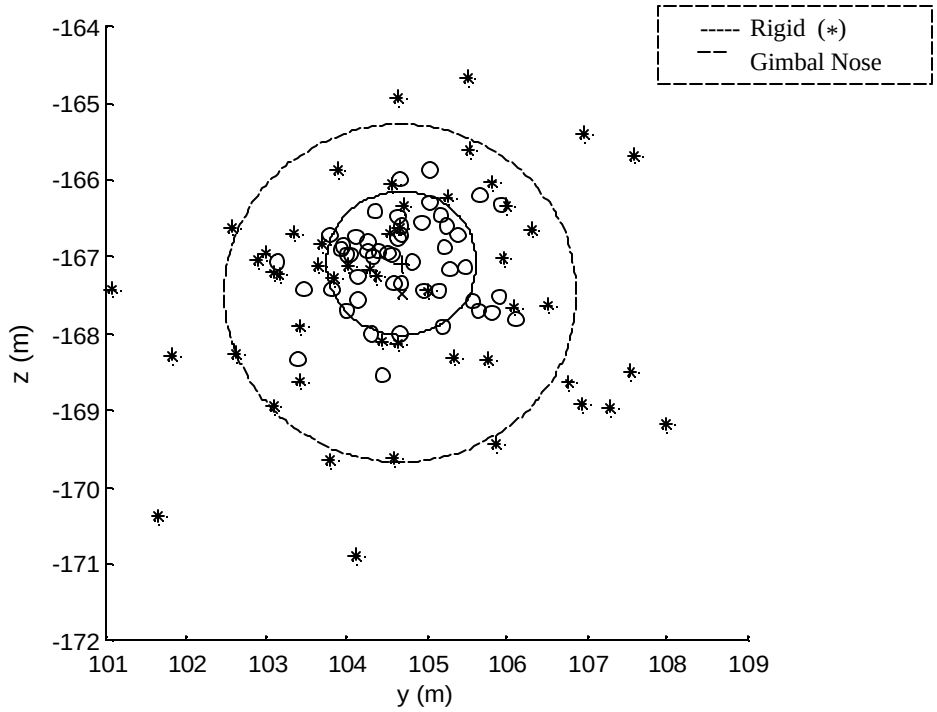

Figure 12. Impact point dispersion at 2 km range.

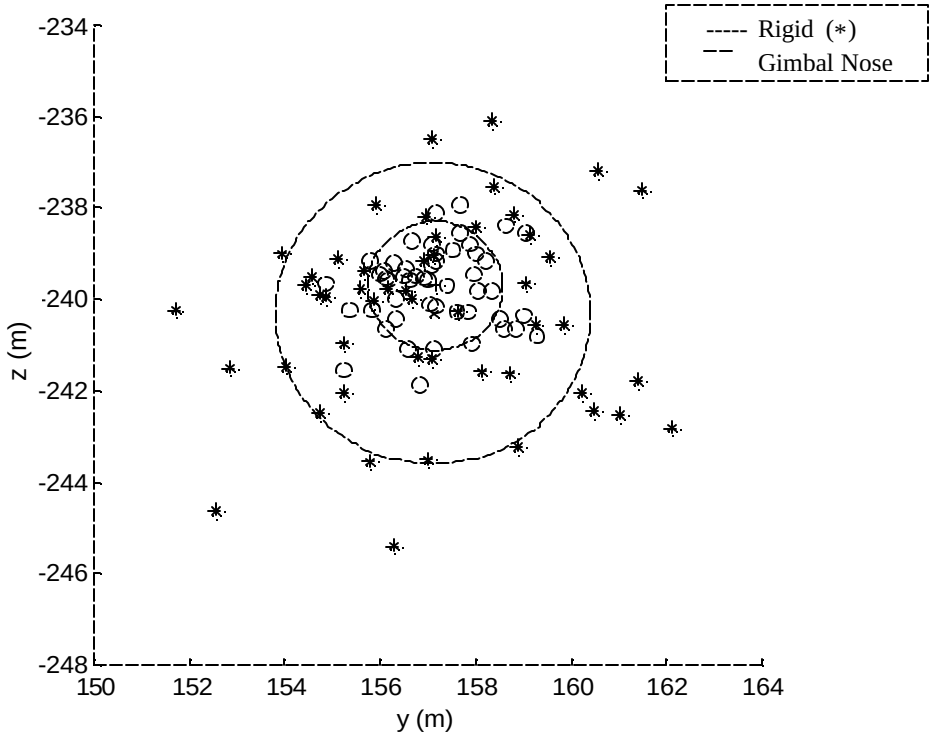

Figure 13. Impact point dispersion at 3 km range.

The impact point charts shown in Figures 11–13 are for a nominal configuration. As shown in Table 1, the baseline gimbal nose configuration has a mass ratio of 0.99, and the gimbal joint is frictionless. Figure 14 investigates how the nose normal force coefficient effects the dispersion radii previously discussed. When the lift coefficient of the nose is zero, the aerodynamic normal load on the projectile is only from the aft body. The impact statistics approach the rigid projectile case, which are shown as diamonds on the chart. A steady decrease in the impact dispersion is realized as the nose normal force coefficient C_{NA}^{F} is increased according to slender body theory C_{NA}^{F} = 2. Figure 15 plots the effect of the mass ratio between the forward and aft projectiles section on impact point dispersion radii. Within practical design limit, the mass ratio between the forward and aft projectile sections does not effect impact point dispersion.

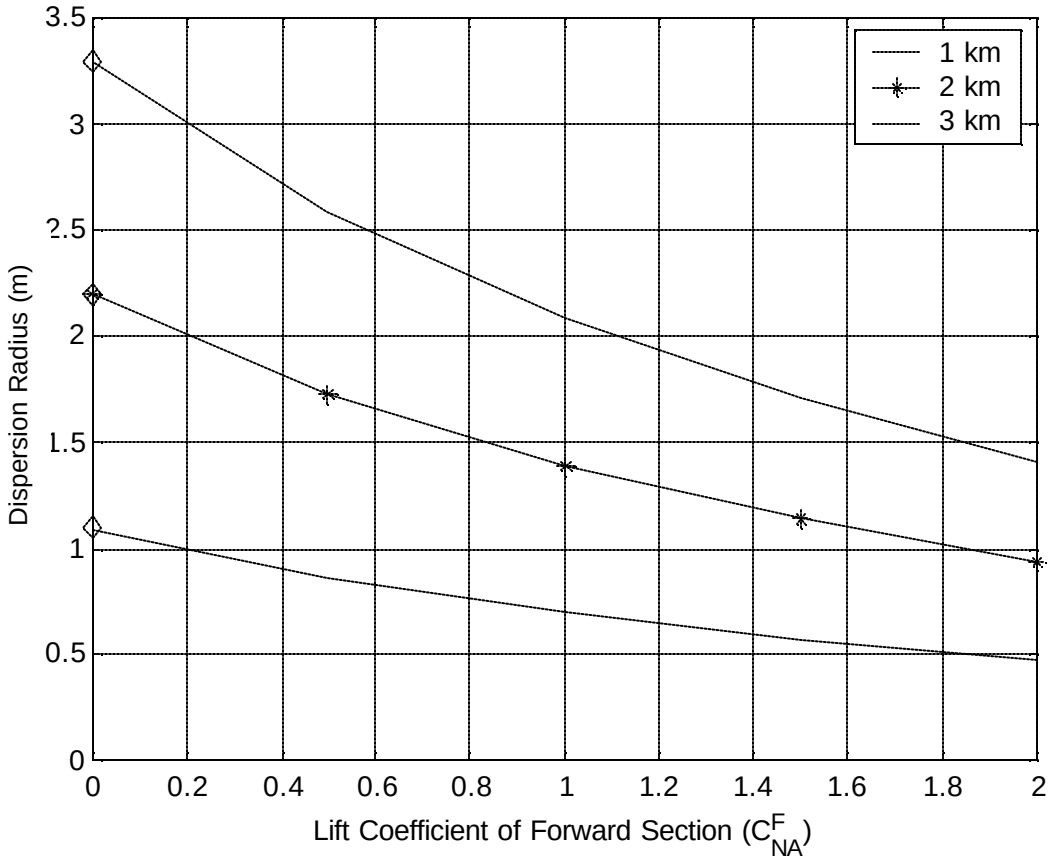

Figure 14. Impact point dispersion vs. nose lift coefficient.

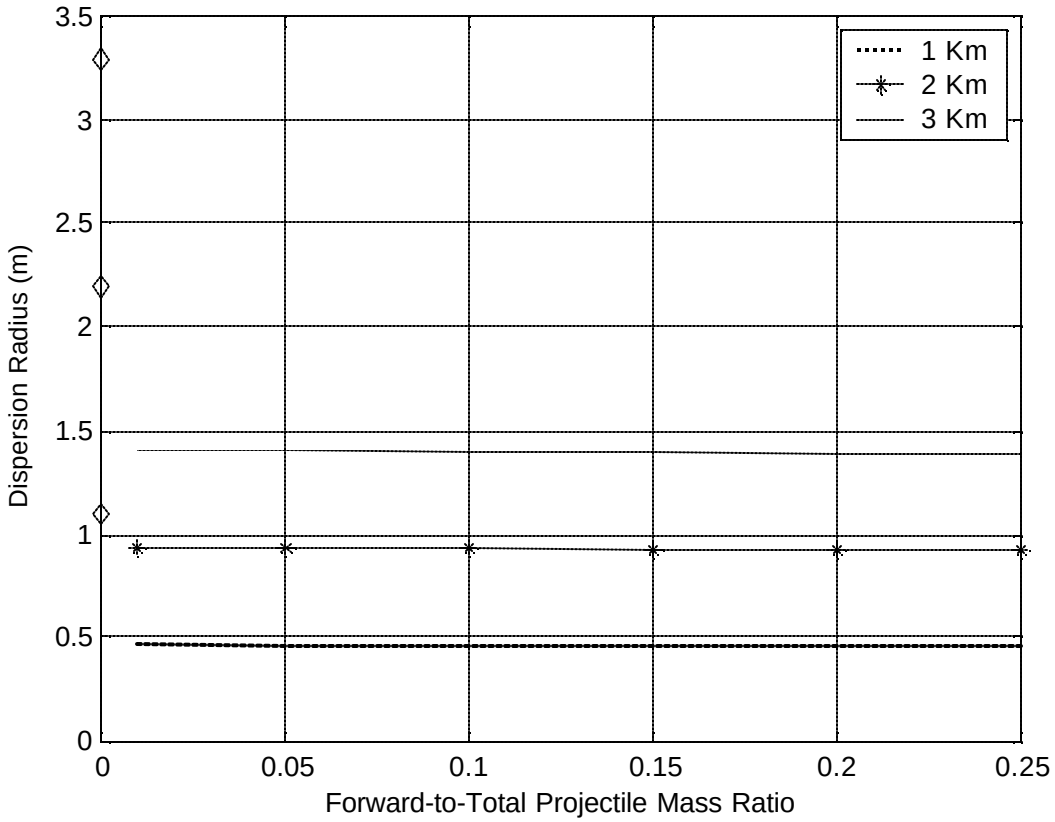

Figure 15. Impact point dispersion vs. forward-to-total mass ratio.

Figure 16 shows the impact point dispersion radii at 1 km, 2 km, and 3 km range as a function of the friction constant C_g. At 1 km and 2 km range, the dispersion radii is an essential constant for all values of C_g. However, at range of 3 km, the dispersion rapidly increases. Since projectile velocity exponentially decreases with range, a critical combination of projectile velocity and damper constant combined to induce large impact point dispersion, which is in fact a much larger dispersion than a similar rigid projectile. The root of this problem is shown in Figures 17 and 18, which plot the position of the tip of the nose of the projectile with respect to the main projectile body. In the case where the gimbal joint is frictionless (Figure 17), the nose initially rotates with relatively large angles and progresses toward a steady state limit cycle of low amplitude. In the case where C_g = 1.0 (Figure 18), the nose angle continuously increases as it approaches the interference limit of total nose deflection of a_g = 5°. Hence, the rotational dynamics of the nose are unstable in this case.

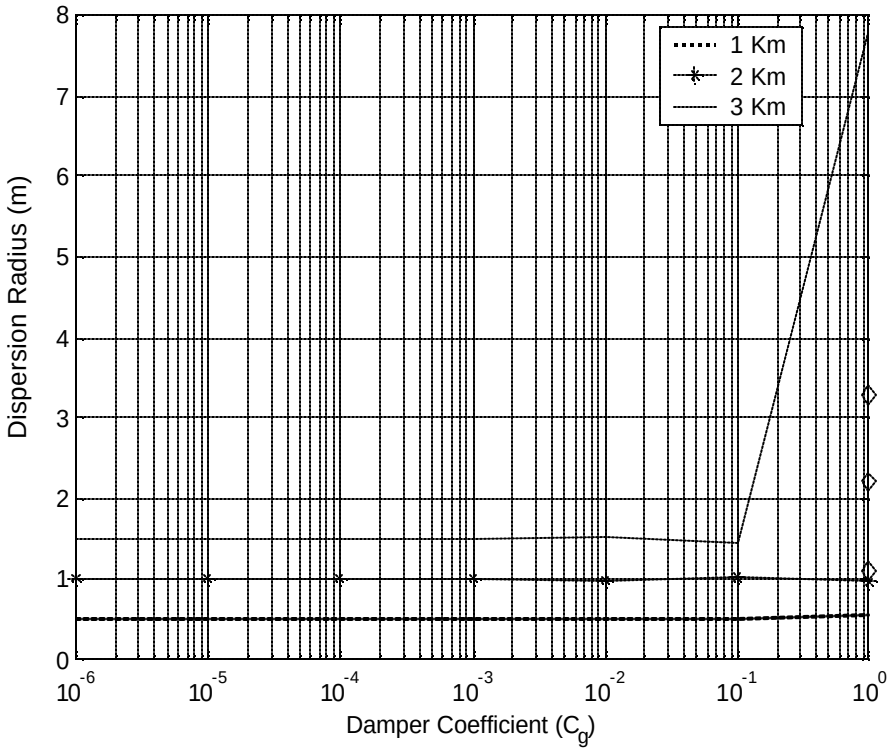

Figure 16. Impact point dispersion vs. gimbal viscous friction coefficient.

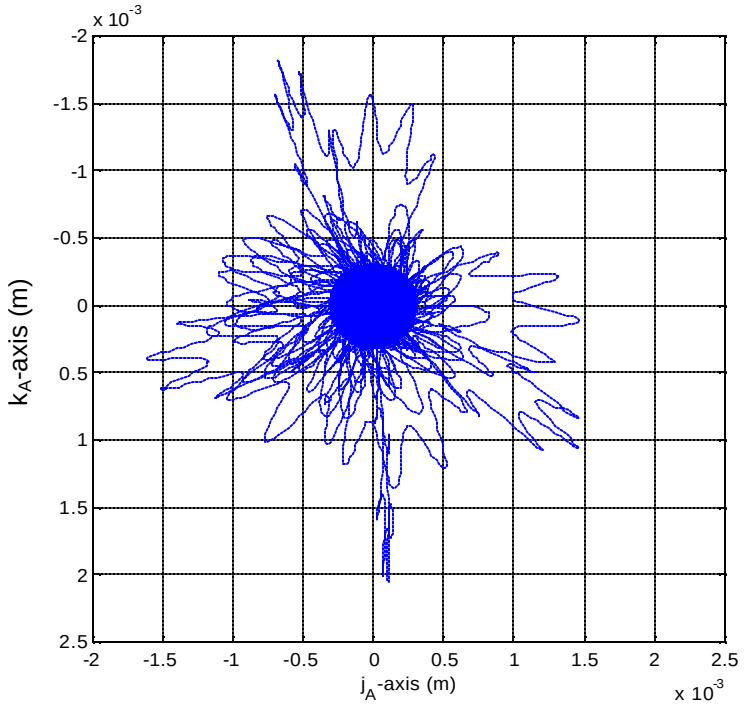

Figure 17. Motion of nose tip with respect to the aft body ($C_g = 0.00$).

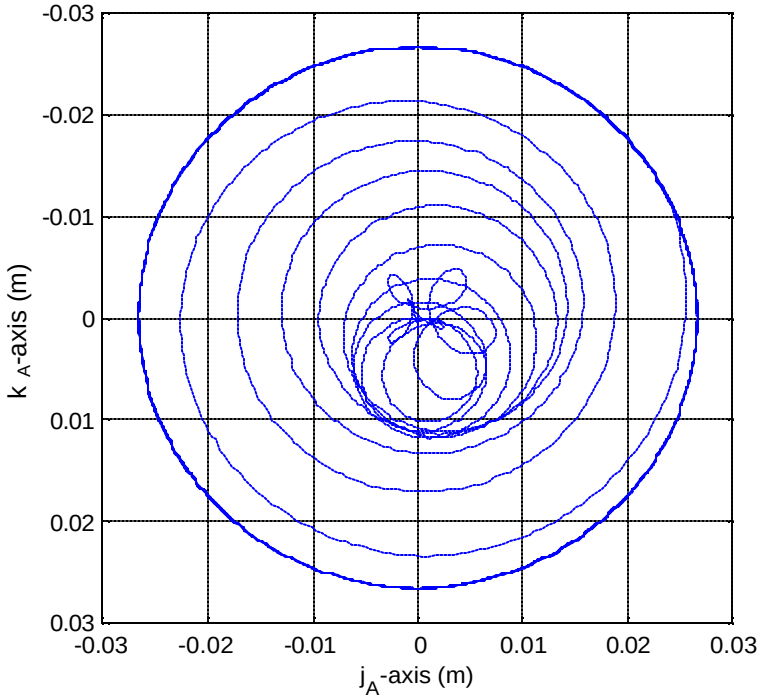

Figure 18. Motion of nose tip with respect to the aft body ($C_g = 1.00$).

4. Conclusion

A penetrator projectile equipped with a gimbal nose wind screen has the potential to drastically reduce impact point dispersion. By mounting the gimbal joint forward of the nose aerodynamic center, the nose tends to turn into the wind, reducing the sensitivity of the trajectory to launch disturbances. In the example case considered, impact point dispersion was reduced by more than 50%. The mean impact point of the rigid and gimbal nose projectile configurations are different. This difference will require fire control system logic to be modified, depending on the particular projectile configuration being launched. Gimbal joint friction is an important design parameter that influences the effectiveness of the gimbal joint to reduce impact point dispersion. For sufficiently large friction in the gimbal joint, the impact point dispersion increases well beyond the dispersion encountered with a rigid body projectile because the nose rotational dynamics are unstable. Hence, the gimbal joint must be designed such that the joint does not degrade as the round sits in long-term storage. Impact point dispersion steadily increases as the nose aerodynamic normal coefficient decreases. Also, dispersion is essentially independent of the mass ratio of the nose and main projectile sections.

INTENTIONALLY LEFT BLANK.

5. References

1. Goddard, R. H. "Apparatus for Steering Aircraft." U.S. Patent 2594766, April 1952.
2. Barrett, R., and J. Stutts. "Modeling, Design, and Testing of a Barrel-Launched Adaptive Munition." Proceedings of the 4th Annual Society of Photo-Optical Engineers Symposium on Smart Structures, San Diego, CA, Society of Photo-Optical Engineers, New York, March 1997.
3. Krantz, W. "High Velocity Aerodynamic Body Having Telescopic Nose Tip." U.S. Patent 4756492, July 1988.
4. Schmidt, E., and W. Donovan. "Technique to Reduce Yaw and Jump of Fin-Stabilized Projectiles." *Journal of Spacecraft and Rockets*, vol. 35, no. 1, pp. 110–111, 1998.
5. Murphy, C. "Free Flight Motion of Symmetric Missiles." U.S. Army Ballistic Research Laboratories, BRLR-1216, Aberdeen Proving Ground, MD, July 1963.
6. Costello, M. F., and D. P. Anderson. "Effect of Internal Mass Unbalance on the Terminal Accuracy and Stability of a Field Artillery Projectile." Proceedings of the 1996 AIAA Atmospheric Flight Mechanics Conference, San Diego, CA, 1996.

SYMBOLS

x, y, z	Components of the position vector of center of mass of the composite body in an inertial reference frame.
u, v, w	Components of the velocity vector of the mass center of the composite body in the aft body reference frame.
f_A, q_A, y_A	Aft body Euler roll, pitch, and yaw angles.
f_F, q_F, y_F	Forward body Euler roll, pitch, and yaw angles.
p_A, q_A, r_A	Components of the angular velocity vector of the aft body in the aft body reference frame.
p_F, q_F, r_F	Components of the angular velocity vector of the forward body in the forward body reference frame.
X, Y, Z	Total external force components on the composite body in the aft body reference frame.
X_A, Y_A, Z_A	Total external force components on the aft body in the aft body reference frame.
X_F, Y_F, Z_F	Total external force components on the forward body in the forward body reference frame.
X_C, Y_C, Z_C	Gimbal joint constraint force components in the aft body reference frame.

L, M, N	Total external moment components on the composite body in the aft body reference frame.
L_A, M_A, N_A	Total external moment components on the aft body in the aft body reference frame.
L_F, M_F, N_F	Total external force components on the forward body in the forward body reference frame.
m_A	Aft body mass.
m_F	Forward body mass.
I_A	Mass moment of inertia matrix of the aft body about the aft body mass.
I_F	Mass moment of inertia matrix of the forward body about the forward body mass center.
$r_{A_X}, r_{A_Y}, r_{A_Z}$	Components of the position vector from the gimbal joint to the mass center of the aft body in the aft body reference frame.
$r_{F_X}, r_{F_Y}, r_{F_Z}$	Components of the position vector from the gimbal joint to the mass center of the forward body in the forward body reference frame.
$\tilde{r}_{F_X}, \tilde{r}_{F_Y}, \tilde{r}_{F_Z}$	Components of the position vector from the gimbal joint to the mass center of the forward body in the aft body reference frame.
C_g	Gimbal joint viscous damping constant.

K_g	Gimbal joint spring constant.
S_A	Aerodynamic reference area for aft projectile section.
S_F	Aerodynamic reference area for forward projectile section.
r	Air density.
a_g	Angle between forward body centerline and aft body center line.
a^*	Dead band angular interference limit between forward and aft section.

REPORT DOCUMENTATION PAGE

Form Approved
OMB No. 0704-0188

1. AGENCY USE ONLY *(Leave blank)*	2. REPORT DATE	3. REPORT TYPE AND DATES COVERED
	April 2001	Final, October 2000 - February 2001

4. TITLE AND SUBTITLE
Improved Dispersion of a Fin-Stabilized Projectile Using a Passive Moveable Nose

5. FUNDING NUMBERS
1L162618.H80

6. AUTHOR(S)
Mark Costello* and Raditya Agarwalla*

7. PERFORMING ORGANIZATION NAME(S) AND ADDRESS(ES)
Oregon State University
Department of Mechanical Engineering
Corvallis, Oregon 97331

8. PERFORMING ORGANIZATION REPORT NUMBER

9. SPONSORING/MONITORING AGENCY NAMES(S) AND ADDRESS(ES)
U.S. Army Research Laboratory
ATTN: AMSRL-WM-BC
Aberdeen Proving Ground, MD 21005-5066

10. SPONSORING/MONITORING AGENCY REPORT NUMBER
ARL-CR-464

11. SUPPLEMENTARY NOTES
*Oregon State University

12a. DISTRIBUTION/AVAILABILITY STATEMENT
Approved for public release; distribution is unlimited.

12b. DISTRIBUTION CODE

13. ABSTRACT *(Maximum 200 words)*

A key and often quoted metric associated with gun systems is impact point accuracy. The extent of impact dispersion is a complex function of a battery of parameters, including gun geometry and tolerances, the fire control system, projectile manufacturing tolerances, etc. The work reported here investigates potential impact point accuracy improvement for a penetrator-type projectile realized by replacing the rigid nose cone wind screen with a passive gimballed nose. By comparing the impact point dispersion of a rigid projectile with a similar gimballed nose projectile, it is shown that impact point accuracy can be significantly improved. For the example penetrator projectile considered, impact point dispersion is reduced by more than 50%.

14. SUBJECT TERMS	15. NUMBER OF PAGES
dispersion, fin-stabilized projectile, nose control	34
	16. PRICE CODE

17. SECURITY CLASSIFICATION OF REPORT	18. SECURITY CLASSIFICATION OF THIS PAGE	19. SECURITY CLASSIFICATION OF ABSTRACT	20. LIMITATION OF ABSTRACT
UNCLASSIFIED	UNCLASSIFIED	UNCLASSIFIED	UL

NSN 7540-01-280-5500

31

Standard Form 298 (Rev. 2-89)
Prescribed by ANSI Std. 239-18 298-102

INTENTIONALLY LEFT BLANK.

NO. OF COPIES ORGANIZATION

2 DEFENSE TECHNICAL INFORMATION CENTER
DTIC OCA
8725 JOHN J KINGMAN RD
STE 0944
FT BELVOIR VA 22060-6218

1 COMMANDING GENERAL
US ARMY MATERIEL CMD
AMCRDA TF
5001 EISENHOWER AVE
ALEXANDRIA VA 22333-0001

1 INST FOR ADVNCD TCHNLGY
THE UNIV OF TEXAS
AT AUSTIN
3925 W BRAKER LN STE 400
AUSTIN TX 78759-5316

1 US MILITARY ACADEMY
MATH SCI CTR EXCELLENCE
MADN MATH
THAYER HALL
WEST POINT NY 10996-1786

1 DIRECTOR
US ARMY RESEARCH LAB
AMSRL D
DR D SMITH
2800 POWDER MILL RD
ADELPHI MD 20783-1197

1 DIRECTOR
US ARMY RESEARCH LAB
AMSRL CS IS R
2800 POWDER MILL RD
ADELPHI MD 20783-1197

3 DIRECTOR
US ARMY RESEARCH LAB
AMSRL CI OK TL
2800 POWDER MILL RD
ADELPHI MD 20783-1197

NO. OF COPIES ORGANIZATION

3 DIRECTOR
US ARMY RESEARCH LAB
AMSRL CS IS T
2800 POWDER MILL RD
ADELPHI MD 20783-1197

ABERDEEN PROVING GROUND

2 DIR USARL
AMSRL CI LP (BLDG 305)

NO. OF COPIES	ORGANIZATION
3	AIR FORCE RSRCH LAB MUNITIONS DIR AFRL / MNAV G ABATE 101 W EGLIN BLVD STE 219 EGLIN AFB FL 32542
1	CDR WL / MNMF D MABRY 101 W EGLIN BLVD STE 219 EGLIN AFB FL 32542-6810
20	OREGON STATE UNIVERSITY DEPT OF MECHL ENGRG M COSTELLO CORVALLIS OR 97331
4	CDR US ARMY ARDEC AMSTA AR CCH J DELORENZO S MUSALI R SAYER P DONADIO PICATINNY ARESENAL NJ 07806-5000
7	CDR US ARMY TANK MAIN ARMAMENT SYSTEM AMCPM TMA D GUZIEWICZ R DARCEY C KIMKER R JOINSON E KOPOAC T LOUZIERIO C LEVECHIA PICATINNY ARESENAL NJ 07806-5000

NO. OF COPIES	ORGANIZATION
1	CDR USA YUMA PROV GRND STEYT MTW YUMA AZ 85365-9103
1	DIR BENET LABORATORIES SMCWV QAR T MCCLOSKEY WATERVLIET NY 12189-5000
10	CDR US ARMY TACOM AMCPEO HFM AMCPEO HFM F AMCPEO HFM C AMCPM ABMS AMCPM BLOCKIII AMSTA CF AMSTA Z AMSTA ZD AMCPM ABMS S W DR PATTISON A HAVERILLA WARREN MI 48397-5000
1	CDR USAOTEA CSTE CCA DR RUSSELL ALEXANDRIA VA 22302-1458
2	DIR US ARMY ARMOR CTR & SCHL ATSB WP ORSA A POMEY ATSB CDC FT KNOX KY 40121
1	CDR US ARMY AMCCOM AMSMC ASR A MR CRAWFORD ROCK ISLAND IL 61299-6000

NO. OF COPIES	ORGANIZATION
2	PROGRAM MANAGER GROUND WEAPONS MCRDAC LTC VARELA CBGT QUANTICO VA 22134-5000
4	COMMANDER US ARMY TRADOC ATCD T ATCD TT ATTE ZC ATTG Y FT MONROE VA 23651-5000
1	NAWC F PICKETT CODE C2774 CLPL BLDG 1031 CHINA LAKE CA 93555
1	NAVAL ORDNANCE STATION ADVNCD SYS TCHNLGY BRNCH D HOLMES CODE 2011 LOUISVILLE KY 40214-5001
1	NVL SRFC WRFR CTR F G MOORE DAHLGREN DIVISION CODE G04 DAHLGREN VA 22448-5000
1	US MILITARY ACADEMY MATH SCI CTR OF EXCELLENCE DEPT OF MATHEMATICAL SCI MDN A MAJ DON ENGEN THAYER HALL WEST POINT NY 10996-1786

NO. OF COPIES	ORGANIZATION
3	DIR SNL A HODAPP W OBERKAMPF F BLOTTNER DIVISION 1631 ALBUQUERQUE NM 87185
3	ALLIANT TECH SYSTEMS C CANDLAND R BURETTA R BECKER 7225 NORTHLAND DR BROOKLYN PARK MN 55428
3	DIR USARL AMSRL SE RM H WALLACE AMSRL SS SM J EIKE A LADAS 2800 POWDER MILL RD ADELPHI MD 20783-1145
1	OFC OF ASST SECY OF ARMY FOR R&D SARD TR W MORRISON 2115 JEFFERSON DAVIS HWY ARLINGTON VA 22202-3911
2	CDR USARDEC AMSTA FSP A S DEFEO R SICIGNANO PICATINNY ARESENAL NJ 07806-5000
2	CDR USARDEC AMSTA AR CCH A M PALATHINGAL R CARR PICATINNY ARESENAL NJ 07806-5000

NO. OF COPIES	ORGANIZATION
5	TACOM ARDEC AMSTA AR FSA K CHIEFA AMSTA AR FS A WARNASCH AMSTA AR FSF W RYBA AMSTA AR FSP S PEARCY J HEDDERICH PICATINNY ARESENAL NJ 07806-5000
5	CDR US ARMY MICOM AMSMI RD P JACOBS P RUFFIN AMSMI RD MG GA C LEWIS AMSMI RD MG NC C ROBERTS AMSMI RD ST GD D DAVIS RSA AL 35898-5247
3	CDR US ARMY AVN TRP CMD DIRECTORATE FOR ENGRNG AMSATR ESW M MAMOUD M JOHNSON J OBERMARK RSA AL 35898-5247
1	DIR US ARMY RTTC STERT TE F TD R EPPS BLDG 7855 REDSTONE ARSENAL AL 38598-8052
2	STRICOM AMFTI EL D SCHNEIDER R COLANGELO 12350 RESEARCH PKWY ORLANDO FL 32826-3276
1	CDR OFFICE OF NAVAL RES J GOLDWASSER CODE 333 800 N QUINCY ST RM 507 ARLINGTON VA 22217-5660

NO. OF COPIES	ORGANIZATION
1	CDR US ARMY RES OFFICE AMXRO RT IP TECH LIB PO BOX 12211 RESEARCH TRIANGLE PARK NJ 27709-2211
4	CDR US ARMY AVN TRP CMD AVIATION APPLIED TECH DIR AMSATR TI R BARLOW E BERCHER T CONDON B TENNEY FT EUSTIS VA 23604-5577
3	CDR NAWC WEAPONS DIV CODE 543400D S MEYERS CODE C2744 T MUNSINGER CODE C3904 D SCOFIELD CHINA LAKE CA 93555-6100
1	CDR NSWC CRANE DIVISION CODE 4024 J SKOMP 300 HIGHWAY 361 CRANE IN 47522-5000
1	CDR NSWC DAHLGREN DIV CODE 40D J BLANKENSHIP 6703 WEST HWY 98 PANAMA CITY FL 32407-7001
1	CDR NSWC J FRAYSEE D HAGEN 17320 DAHLGREN RD DAHLGREN VA 22448-5000

NO. OF COPIES	ORGANIZATION
5	CDR NSWC INDIAN HEAD DIV D GARVICK CODE 40D L FAN CODE 4110C V CARLSON CODE 4120 H LAST CODE 4140E T GRIFFIN CODE 450D 101 STRAUSS AVE INDIAN HEAD MD 20640-5000
1	CDR NSWC INDIAN HEAD DIV LIBRARY CODE 8530 BLDG 299 101 STRAUSS AVE INDIAN HEAD MD 20640
2	US MILITARY ACADEMY MATH SCI CTR OF EXCELLENCE DEPT OF MATHEMATICAL SCI MDN A MAJ D ENGEN R MARCHAND THAYER HALL WEST POINT NY 10996-1786
3	CDR US ARMY YUMA PG STEYP MT AT A A HOOPER STEYP MT EA YUMA AZ 85365-9110
6	CDR NSWC INDIAN HEAD DIV CODE 570D J BOKSER CODE 5710 L EAGLES J FERSUSON CODE 57 C PARIS CODE 5710G S KIM CODE 5710E S JAGO 101 STRAUSS AVE ELY BLDG INDIAN HEAD MD 20640-5035
1	BRUCE KIM MICHIGAN STATE UNIVERSITY 2120 ENGINEERING BLDG EAST LANSING MI 48824-1226

NO. OF COPIES	ORGANIZATION
2	INDUSTRIAL OPERATION CMD AMFIO PM RO W MCKELVIN MAJ BATEMAN ROCK ISLAND IL 61299-6000
3	PROGRAM EXECUTIVE OFFICER TACTICAL AIRCRAFT PROGRAMS PMA 242 1 MAJ KIRBY R242 PMA 242 33 R KEISER (2 CPS) 1421 JEFFERSON DAVIS HWY ARLINGTON VA 22243-1276
1	CDR NAVAL AIR SYSTEMS CMD CODE AIR 471 A NAKAS 1421 JEFFERSON DAVIS HWY ARLINGTON VA 22243-1276
4	ARROW TECH ASSOCIATES INC R WHYTE A HATHAWAY H STEINHOFF 1233 SHELBOURNE RD SUITE D8 SOUTH BURLINGTON VT 05403
3	US ARMY AVIATION CTR DIR OF COMBAT DEVELOPMENT ATZQ CDM C B NELSON ATZQ CDC C T HUNDLEY ATZQ CD G HARRISON FORT RUCKER AL 36362

NO. OF COPIES ORGANIZATION

ABERDEEN PROVING GROUND

3 CDR
USA ARDEC
AMSTA AR FSF T
R LIESKE
J WHITESIDE
J MATTS
BLDG 120

1 CDR
USA TECOM
AMSTE CT
T J SCHNELL
RYAN BLDG

3 CDR
USA AMSAA
AMXSY EV
G CASTLEBURY
R MIRABELLE
AMXSY EF
S MCKEY

49 DIR USARL
AMSRL WM
I MAY
T ROSENBERGER

ABERDEEN PROVING GROUND

AMSRL WM BA
W HORST JR
W CIEPELLA
F BRANDON
T BROWN (5 CPS)
L BURKE
J CONDON
B DAVIS
T HARKINS (5 CPS)
D HEPNER
V LEITZKE
M HOLLIS
A THOMPSON
G BROWN

NO. OF COPIES ORGANIZATION

ABERDEEN PROVING GROUND

AMSRL WM BB
B HAUG
OS
J SAHU
M BUNDY
K SOENCKSEN
D LYON
AMSRL WM BC
P PLOSTINS (4 CPS)
G COOPER
B GUID
AMSRL WM BC
J BENDER
J NEWILL
J GARNER
V OSKAY
S WILKERSON
W DRYSDALE
R COATES
A MIKHAL
J WALL
AMSRL WM BD
B FORCH
AMSRL WM BE
M SCHMIDT
AMSRL WM BF
J LACETERA
P HILL
AMSRL WM BR
C SHOEMAKER
J BORNSTEIN